JOURNAL OF AIRCRAFT
Vol. 34, No. 6, November–December 1997

In-Flight Boundary-Layer State Measurements on a High-Lift System: Slat

C. P. van Dam* and S. M. Los†
University of California, Davis, Davis, California 95616
S. J. Miley‡
Old Dominion University, Norfolk, Virginia 23508
V. E. Roback§ and L. P. Yip¶
NASA Langley Research Center, Hampton, Virginia 23681
A. Bertelrud**
Analytical Services and Materials, Inc., Hampton, Virginia 23666
and
P. M. H. W. Vijgen††
High Technology Corporation, Hampton, Virginia 23666

Flight experiments on NASA Langley Research Center's B737-100 airplane were conducted to document flow characteristics for further understanding of high-lift flow physics. The measurements included surface pressure distributions measured using flush pressure taps and pressure belts on the slats, main element, and flap elements, and boundary-layer state changes measured using hot-film anemometry and infrared thermography. In this paper, results obtained in the final phase of flight experiments are presented and analyzed. The analysis primarily focuses on changes in the boundary-layer state measured on the slat as a result of changes in flap setting and/or flight condition. The measurements show that extended runs of laminar flow exist on the slat at relevant angles of attack. Flow mechanisms that affect the extent of laminar flow include attachment-line contamination, crossflow instability, and relaminarization.

Nomenclature

C_p = pressure coefficient, $(p - p_\infty)/q_\infty$
$\bar{c}$ = mean aerodynamic chord, 11.20 ft
c_n = chord length normal to leading edge
f = frequency of flow instability, Hz
h_p = pressure altitude, ft
K = relaminarization parameter
M_∞ = freestream Mach number
n = amplification factor of flow instability
p = local static pressure, psf
p_∞ = freestream static pressure, psf
q_∞ = freestream dynamic pressure, psf
R_{bar} = attachment-line Reynolds number
$R_{\bar{c}}$ = Reynolds number, $V_\infty \bar{c}/\nu$
s = surface distance, ft
$(s_n/c_n)_{al}$ = nondimensional location of attachment line normal to leading edge
t = time, s
V_∞ = true airspeed, ft/s
x/c = nondimensional chordwise coordinate
z/c = nondimensional thickness coordinate
α = airplane angle of attack, deg
δ_f = flap setting, deg
Λ = wing sweep angle, deg
ν = kinematic viscosity, ft^2/s

Presented as Paper 95-3911 at the AIAA 1st Aircraft Engineering, Technology, and Operations Congress, Los Angeles, CA, Sept. 19–21, 1995; received Jan. 16, 1997; revision received May 27, 1997; accepted for publication May 30, 1997.

*Professor, Department of Mechanical and Aeronautical Engineering. E-mail: cpvandam@ucdavis.edu. Senior Member AIAA.
†Graduate Student, Department of Mechanical and Aeronautical Engineering.
‡Senior Research Associate. Senior Member AIAA.
§Aerospace Technologist. Member AIAA.
¶Senior Research Engineer. Associate Fellow AIAA.
**Principal Scientist. Senior Member AIAA.
††R&D Engineer; currently Senior Specialist Engineer, Boeing Commercial Airplane Group, Seattle, WA 98124. Senior Member AIAA.

Introduction

THE design of subsonic civil transport airplanes is, to a large extent, governed by the takeoff and landing requirements in combination with aerodynamic performance characteristics of the airplane at low-speed, high-lift conditions. Accurate prediction of these aerodynamic performance characteristics for a given multielement high-lift configuration remains challenging, mainly because of the complex flows and the lack of a complete description and understanding of these flows. The complexity comes, in part, from the multielement geometry, but to a greater extent it comes from the viscous effects that govern these flow characteristics. Since these flows are sensitive to changes in Reynolds number, the prediction of a full-scale aerodynamic performance based on wind-tunnel results obtained at lower Reynolds numbers remains difficult, because it requires complete understanding of the scaling principles. Prediction of the full-scale aerodynamic performance from computational aerodynamic codes is still far from accurate because of deficiencies in modeling of the high-lift flow physics, as well as limitations in computer hardware.

This lack of capabilities in the prediction of a high-lift aerodynamic performance at full-scale Reynolds numbers was partially responsible for the development of high-Reynolds-number wind tunnels[1] as well as the need for a set of detailed experimental data measured in flight at full-scale conditions. A limited set of flight data at high-lift conditions was obtained on the Airbus A310 transport aircraft.[2,3] In response to the need

for a more complete data set for flows about multielement configurations at full-scale high-lift conditions, a multiphased research project on the NASA Transport Systems Research Vehicle (TSRV), a B737-100 airplane, was conducted. In phase I of the project, exploratory experiments including surface-pressure measurements using pressure belts and flow-separation measurements using Preston tubes were conducted on the research airplane's triple-slotted Fowler flap system.[4] In phase II, more detailed flow measurements were conducted using pressure belts and Preston tubes across the full chord at the 58% semispan station of the starboard wing.[5,6] These results were also used to determine the instrumentation layout of the expanded phase III flight experiments. In phase III, the slats, main element, spoilers, and flaps on the aircraft starboard wing, outboard of the engine, were instrumented with approximately 1000 pressure ports (including static and total) and 100 hot-film sensors. In-flight measurements included surface pressures, shear-layer velocity profiles, surface shear stresses, hot-film anemometry, and infrared (IR) imaging for the detection of changes in boundary-layer state, aeroelastic deformations, and flow visualization. Phase III flights were conducted in 1994, and an overview of the experiments and overall results is given by Yip et al.[7]

The purpose of this series paper is to discuss the results of an analysis of the boundary-layer state changes that were observed on the slat. A companion paper discusses boundary-layer state changes that were observed on the main element and foreflap during the phase III flights.[8] Specifically, such changes include attachment-line transition, relaminarization, crossflow transition, and contamination of laminar flow by the wakes of upstream elements.

Flight Experiment and Instrumentation

High-lift flight experiments were conducted on NASA Langley Research Center's TSRV, a Boeing B737-100 airplane. The airplane has been modified extensively for research in flight systems, flight operations, and flight mechanics. The modifications include a rear flight deck that is supported by several computers to provide digital flight control and can be used to maintain a variety of flight parameters at specified conditions. The primary mode of operation during these high-lift experiments was piloting the airplane from the rear (research) flight deck, which resulted in very stable flight conditions and allowed the attainment of specified conditions with a high degree of accuracy.

The Boeing B737-100 TSRV is a twin-jet, short-haul, subsonic transport designed to cruise at approximately Mach 0.78. The airplane wing incorporates a five-element high-lift system to allow operation from relatively short runways. The high-lift system includes a leading-edge device (Krüger flap inboard of the engine and slat outboard), which deploys in conjunction with the triple-slotted flaps. The airplane has a wingspan of 93 ft, an aspect ratio of 8.82, and a wing leading-edge sweep angle (outboard of the engine) of 27.5 deg. The present investigation focused on documenting the flow characteristics of the starboard wing outboard of the engine. The high-lift system of this wing section includes the following five elements: the segmented slat, main element, foreflap, midflap, and the aft flap. The three slat segments on the starboard wing are designated (from inboard to outboard) slat nos. 4, 5, and 6 (Fig. 1). Slat no. 4 of the TSRV has two settings: retracted and extended. The other two slats move in unison with slat no. 4 for flap settings smaller than about 25 deg. For flap settings beyond the 25-deg setting, the two outboard slats extend fully to a third, more nose-down setting. Therefore, for flap settings above 25 deg, a spanwise planform break exists between slat nos. 4 and 5, as depicted in Fig. 1. The surface of the high-lift elements was filled and smoothed. Also, before each flight, the surface was cleaned to remove any insect debris or other surface contamination. The test conditions included steady flight and slowly decelerating (<1 kn/5 s) flight at altitudes

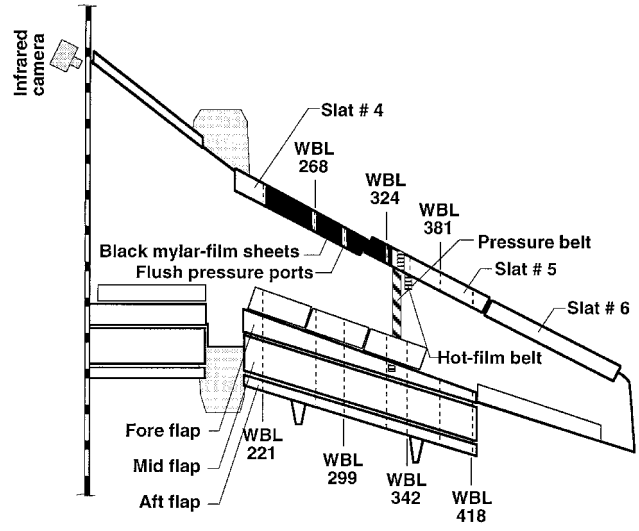

Fig. 1 Layout of pertinent instrumentation on starboard wing of NASA TSRV (B737-100). Wing depicted in the landing configuration ($\delta_f > 25$ deg).

ranging from 5000 to 20,000 ft, airspeeds from flap placard speed to stall onset, and flap settings from 5 to 40 deg. Comparisons between results obtained in steady level flight and slowly decelerated flight have shown no discernible effects of the small deceleration.

An overview of the pertinent instrumentation is provided in Fig. 1. The measurements included surface pressures using flush ports on the slats and trailing-edge flaps, surface pressures using belts on the main element, and detection of boundary-layer state changes using surface hot-film anemometry and infrared thermography. The emphasis of the present paper is on the boundary-layer state data on the slat. For this reason, only the hot-film anemometer system and the infrared imaging system are described in some detail. The pressure measurement system is described in Ref. 7. Based on the method of Kline and McClintock,[9] the uncertainty in C_p is calculated to be approximately ± 0.088. Repeatability studies based on data measured during different flights typically showed smaller discrepancies in C_p. The uncertainty in the measured airplane parameters, e.g., α, is discussed in Ref. 7.

An anemometer system was used to acquire high-frequency ($\approx$50 kHz) hot-film signals. A total of 98 hot-film sensors were multiplexed to two seven-channel Dantec constant-temperature anemometer systems generating analog output signals. All hot-film channels were digitized via a high-speed analog-to-digital signal converter and stored on a high-capacity tape storage unit. The analog output signals of the anemometers were also displayed on 14 minioscilloscopes mounted on the experimenter's instrumentation rack located in the airplane cabin. This instrumentation rack also housed the workstation that performed the digital hot-film data acquisition, displayed the digital data, and allowed the experimenter to select two hot-film sensor banks (each bank containing seven sensors) from which to acquire simultaneous data. In the overview paper by Yip et al.,[7] only fluctuating ac voltage outputs of the anemometers stored on tape using FM signal processing are presented. In the present paper as well as in Ref. 8, the separately stored complete (ac and dc) digital output signals of the anemometers are presented and discussed. The main advantage of the latter representation is that shifts in the dc or mean value can provide additional information about the flow physics.

The majority of the 98 hot-film sensors were arranged on hot-film belts to minimize flow interference. Individual sensors consisted of a layer of nickel (sensor thickness = 6–7 μin., width = 0.003 in., length = 0.060 in.) deposited on a flexible polyimide film (thickness = 0.002 in.) substrate. A protective

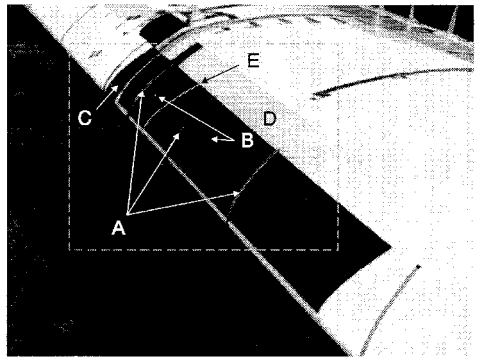

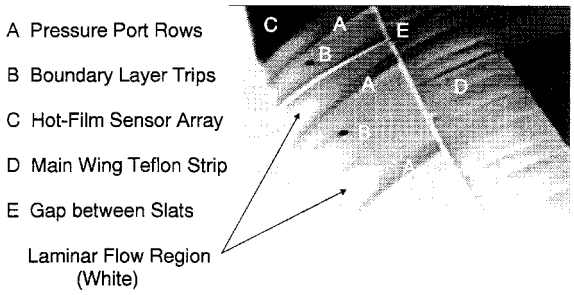

Fig. 2 IR imager viewing area (top) and sample IR image (bottom) including identification of features in image.

coating of aluminum oxide (thickness ~10 μin.) was applied to the sensors. Each sensor had a pair of leads, a layer of nickel plus copper (total thickness ~500 μin.) deposited on the polyimide substrate, geometrically sized to ensure uniform electrical resistance. The polyimide film containing both the sensors and their leads was attached to the aircraft surface using a 0.002-in.-thick layer of adhesive. The edges of the film were then carefully smoothed to prevent premature boundary-layer transition. Each sensor, including leads and cables, had a total resistance of nominally 16 Ω at ambient conditions with an overheat ratio of approximately 1.4 applied to the sensor. Backup sensors including leads were deposited next to most sensors to reduce the need for belt replacements caused by sensor failure. Because the sensors were not individually calibrated, their signals can only be compared qualitatively.

A total of 35 hot-film sensors were located on slat no. 5. Most of these sensors were arranged in the chordwise direction near the 58% semispan station of the starboard wing. However, 14 sensors on the slat were arranged covering the entire span of slat no. 5. The latter sensors were located on the lower surface just ahead of the slat heel. Cables were attached to the leads at a hot-film belt's trailing or outboard edge and were of equal length to ensure cable electronic uniformity necessary for sensor multiplexing. These cables were routed from the hot-film belts to the anemometers in the fuselage of the airplane via the main-element cove to minimize flow interference effects.

An IR imaging system was utilized to visualize global transition patterns as in other (cruise) flight experiments.[10,11] This system, which included a camera and a control unit, was mounted inside the fuselage (Fig. 1) and is described in more detail by Crowder.[12] The camera was mounted in a window blank near the leading edge of the starboard wing at an angle approximately identical to the leading-edge sweep angle of the outboard wing panel (Fig. 1). The camera operates in the wavelength range of 8–12 μm and incorporates a 3X telescope for examining distant targets. The images were monitored real-time onboard the airplane and recorded on videotape for post-flight analysis. In Fig. 2, the IR viewing area is shown along with an explanation of the features in a sample IR image. Thin black mylar sheets, used for enhanced IR signature, were ap-

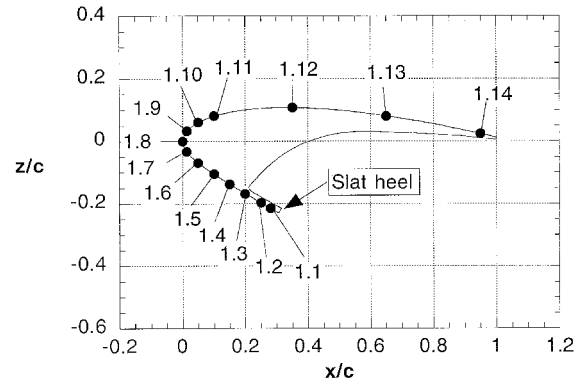

Fig. 3 Location of hot-film sensors on slat.

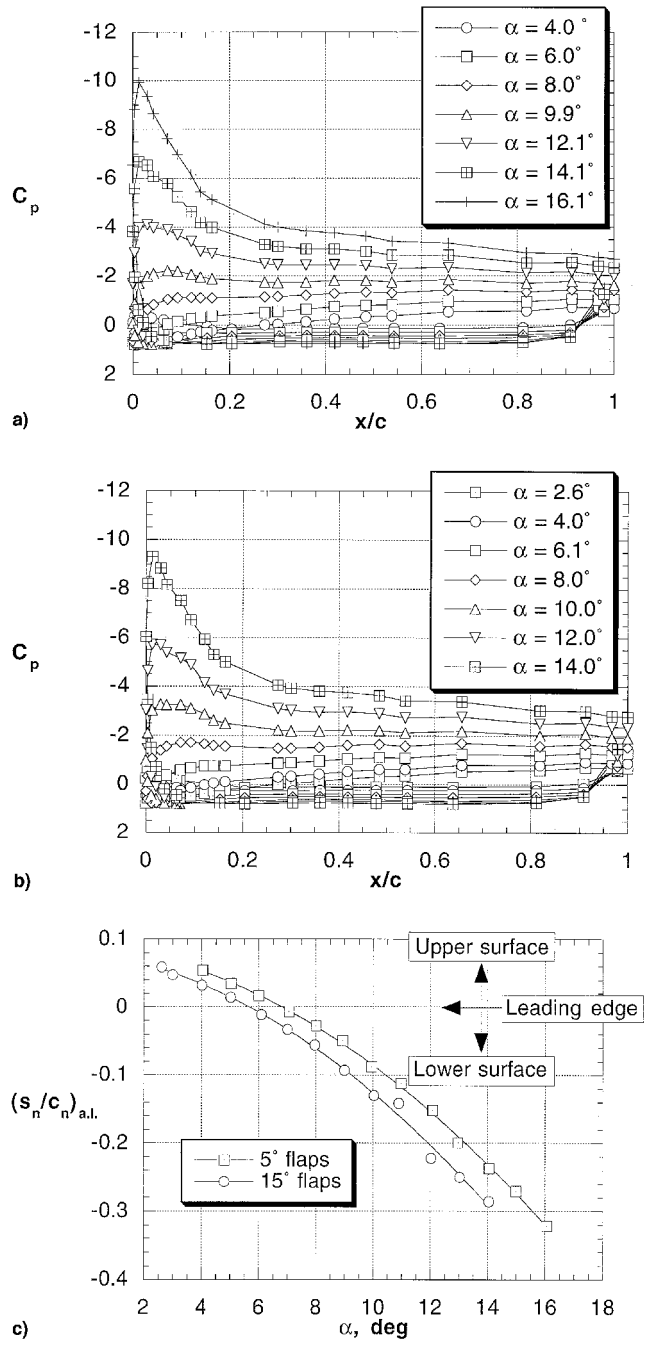

Fig. 4 Pressure distributions and attachment-line location at WBL 324 (h_p = 5000 ft): a) 5-deg flaps, b) 15-deg flaps, and c) effect of α and δ_f on attachment-line location.

plied to the outboard spanwise portion of slat no. 4 and the inboard spanwise portion of slat no. 5. Note that the sheets neither covered the rows of pressure ports nor the break between slats nos. 4 and 5. More information regarding the IR boundary-layer transition technique and the results obtained with this technique in the present experiment can be found in Ref. 13. Although comparison between hot-film results with and without mylar sheets did not indicate an effect of the sheets on the boundary-layer state changes discussed in this paper, the hot-film anemometry measurements presented herein were obtained during flights without mylar sheets on the slat.

Slat Transition Results

Boundary-layer state measurements for the slats using the previously described anemometer and IR systems have been analyzed and are presented and discussed in this paper. The measurements included transition of the upper surface flow at low angles of attack, transition of the attachment-line boundary layer from the laminar to the turbulent state at high angles of attack, and the subsequent apparent relaminarization of the flow in the highly curved leading-edge region of the slat. The analysis focuses on the slats in takeoff position for two reasons: 1) the airplane is able to fly at higher angles of attack and faster for lower flap settings,[5,6] thereby increasing the attachment-line Reynolds number, and 2) the reduced slat deflection angle maximized the quality of the IR images.

In Fig. 3, the slat geometry near WBL 324 is depicted and the location of the hot-film sensors just outboard of this station is marked. Most of the sensors were located along the lower surface ahead of the slat heel. The pressure distributions measured at wing-butt-line (WBL) 324 for the slat in the takeoff position are depicted in Figs. 4a and 4b for the 5- and 15-deg flap setting, respectively (see Refs. 6 and 7 for additional slat pressure distributions). The pressure distributions for the two flap settings are nearly identical except for a shift of approximately 1.5 deg in the corresponding angle of attack. In Fig. 4c, the position of the slat attachment line (maximum-pressure point) is plotted as function of α for the two takeoff flap settings. The attachment-line paths are nearly identical except for the α-shift of approximately 1.5 deg. At low angles of attack, the attachment line was on the upper surface and, consequently, the suction peak occurred on the lower surface leading to transition governed by Tollmien–Schlichting/inflectional instability just downstream of the peak on the lower surface. In Fig. 5, hot-film data measured along the slat during the initial part of a slow deceleration with $\delta_f = 15$ deg are shown as a function of time over a 39-s window. At the beginning of this sequence, $\alpha = 2.6$ deg ($M_\infty = 0.315$, $R_{\bar{c}} = 21.8 \times 10^6$) and the flow along the lower surface (sensors 1.1–1.5) and along the aft portion of the upper surface (sensors 1.13 and 1.14) was turbulent. At this point, the low-amplitude signal indicated laminar flow in the leading-edge region (sensors 1.6–1.11) and the high-amplitude signal at sensor 1.12 indicated intermittent changes in the boundary-layer state associated with transition. At $\alpha = 2.6$ deg, the attachment line was located near sensor 1.9 and moved toward the leading edge with increasing angle of attack. The slow deceleration and the ensuing increase in angle of attack resulted in a reduction in the suction peak on the lower surface and a flattening of the adverse pressure gradient downstream of the peak. As a result, at the end of the sequence depicted in Fig. 5 ($\alpha = 3.1$ deg, $M_\infty = 0.305$, $R_{\bar{c}} = 21.1 \times 10^6$), the flow at sensor 1.5 became laminar. In the favorable pressure-gradient flow along the upper surface,

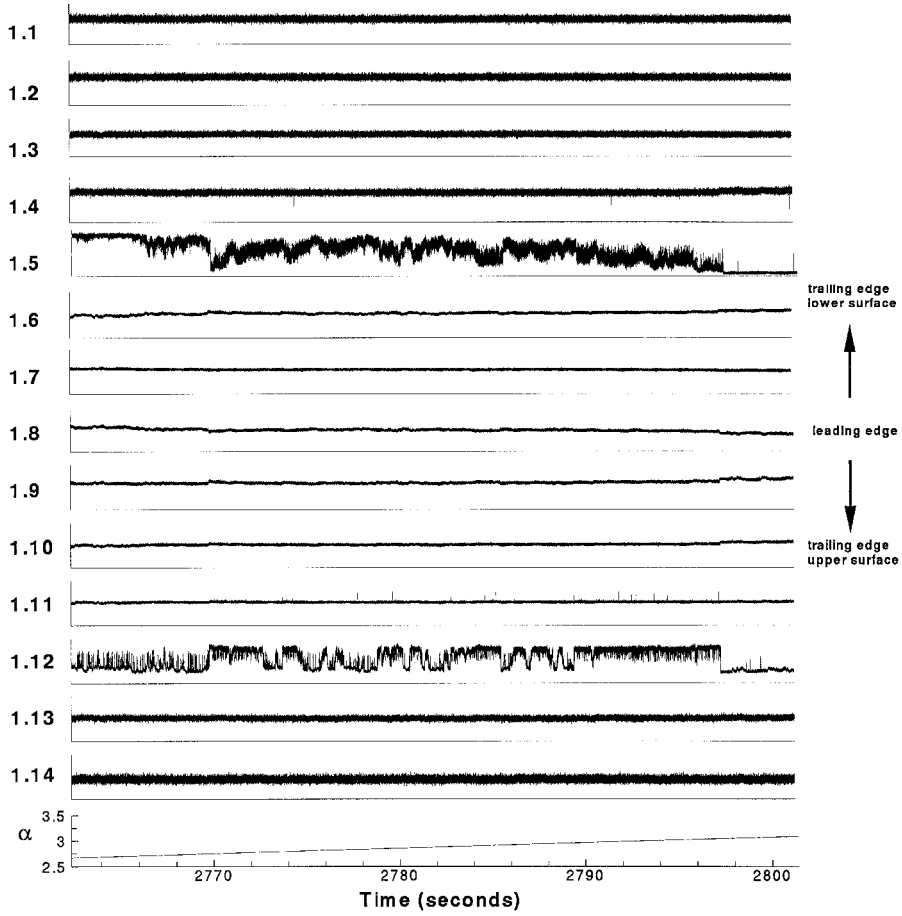

Fig. 5 Hot-film results (digital) depicting boundary-layer state changes on slat during slow deceleration (15-deg flaps, $h_p = 5000$ ft). Segment starts at $t = 2762$ s, $\alpha = 2.6$ deg, $M_\infty = 0.315$, $R_{\bar{c}} = 21.8 \times 10^6$, and ends at $t = 2801$ s, $\alpha = 3.1$ deg, $M_\infty = 0.305$, $R_{\bar{c}} = 21.1 \times 10^6$. Vertical scale range is identical for all sensors.

crossflow instability caused transition ahead of the slat trailing edge as indicated by the hot-film signals for sensors 1.12 (transitional) and 1.13 and 1.14 (turbulent) in Fig. 5, and the limited white-colored (laminar) regions in the IR image of the slat obtained at similar conditions and $\alpha = 2.9$ deg (Fig. 6a). For the 5-deg flap setting, the attachment line moved from the upper surface to the lower surface at $\alpha = 7$ deg (Fig. 4c), and the pressure gradient along the upper surface remained favorable until $\alpha \approx 9$ deg (Fig. 4a). At 15-deg flaps, the attachment line changed surfaces at $\alpha = 5.5$ deg (Fig. 4c) and the pressure gradient remained favorable until $\alpha \approx 7.5$ deg (Fig. 4b). In this range of angles of attack, the upper surface of the slat was completely laminar as shown by the extended white-colored regions at $\alpha = 5.9$ deg in Fig. 6b. With increasing angle of attack, the leading-edge suction peak (now on the upper surface) grew rapidly, causing loss of laminar flow along the upper surface as shown by the limited white-colored regions at $\alpha = 9.0$ deg in Fig. 6c. Simultaneously, on the lower surface, the attachment line moved away from the highly curved leading edge toward the nearly flat slat heel.

In Fig. 7, hot-film data measured along the slat during the latter part of the deceleration with $\delta_f = 5$ deg are shown as a function of time over a 44-s window. At the beginning of this sequence, $\alpha = 13.8$ deg ($M_\infty = 0.209$, $R_{\bar{c}} = 14.5 \times 10^6$), and the flow along the upper surface downstream of the suction peak (sensors 1.11–1.14) was turbulent, whereas the flow along the lower surface and the leading-edge region of the upper surface was laminar except for a small region just upstream of the slat heel. Near the slat heel, the flow was affected by the unsteadiness in the separated cove flow, as indicated by the high-amplitude low-frequency signal of sensor 1.1 (see Fig. 17 in Ref. 2 indicating a similar unsteadiness of the flow near the slat heel). At $\alpha = 13.8$ deg, the attachment line was located between sensors 1.3–1.4 and moved away from the highly curved leading edge (toward sensor 1.1) with increasing angle of attack. Contamination triggered transition onset at $\alpha = 13.9$ deg, when turbulent bursts appeared on the attachment line. These flow disturbances convect streamwise where they register on the hot-film sensors on both sides of the attachment line (see signals of sensors 1.1–1.6 in Fig. 7). The lower surface pressure gradient is favorable toward the leading edge, and the turbulent spots are damped as a result. Eventually, in the highly accelerated flow around the leading edge, the turbulent disturbances appear to disappear (sensors 1.7–1.9). At the end of the sequence depicted in Fig. 7, $\alpha = 15.9$ deg ($M_\infty = 0.199$, $R_{\bar{c}} = 13.7 \times 10^6$), and the attachment line (as determined from the pressure measurements) was located near sensor 1.2.

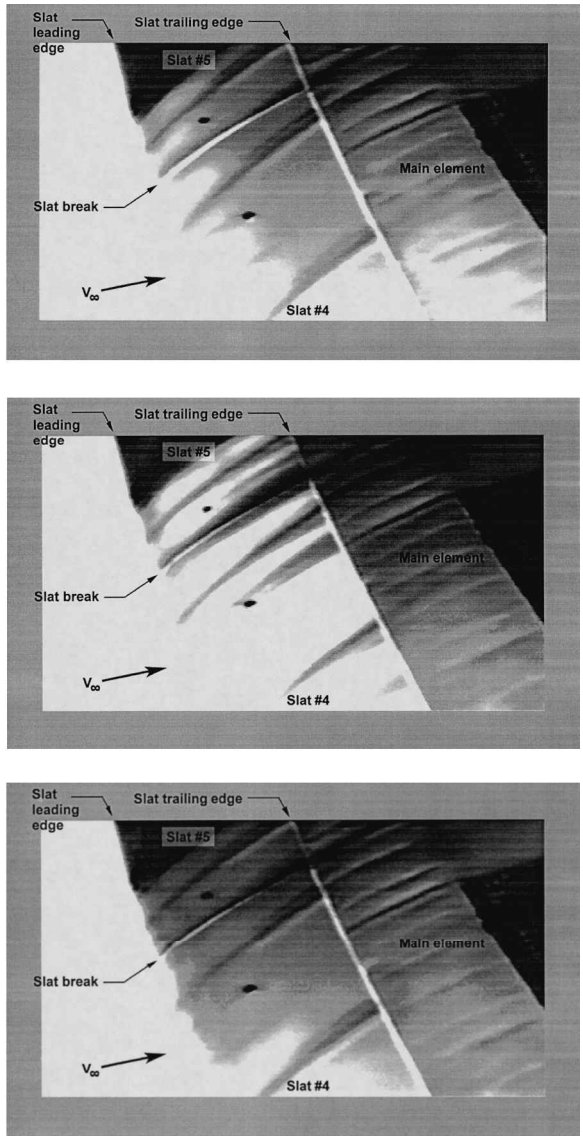

Fig. 6 IR images depicting laminar boundary-layer flow along upper surface of slats (15-deg flaps, h_p = 10,000 ft): a) $\alpha = 2.9$ deg, $M_\infty = 0.331$, $R_{\bar{c}} = 19.0 \times 10^6$; b) $\alpha = 5.9$ deg, $M_\infty = 0.277$, $R_{\bar{c}} = 15.9 \times 10^6$; and c) $\alpha = 9.0$ deg, $M_\infty = 0.239$, $R_{\bar{c}} = 13.7 \times 10^6$.

Discussion

The boundary-layer state of a swept lifting surface is dependent on the state of the attachment-line boundary layer. At high-lift conditions, a change from laminar to turbulent attachment-line flow and the associated changes in the development of the boundary layer on the lifting surface downstream of the attachment line can have a significant effect on the maximum-lift performance of the configuration, as demonstrated by Woodward et al.[14] and Meredith[15] in wind-tunnel experiments. An important parameter when studying the transition characteristics of the attachment-line boundary layer is the attachment-line Reynolds number, $R_{\text{bar}} = W_\infty \kappa/\nu$, where $W_\infty = V_\infty \sin \Lambda$ is the spanwise component of the freestream velocity, and $\kappa = (\nu/U'_n)^{-0.5}$ is the characteristic length. The quantity, U'_n, represents the inviscid velocity gradient at the attachment line in the direction normal to it. Gaster,[16] Pfenninger,[17] and Poll[18] provide additional information on the attachment-line Reynolds number. Their studies, among others, have shown that for $R_{\text{bar}} < 245$, the attachment-line boundary layer will tend to remain laminar, and turbulent contamination introduced in the boundary layer by significant surface roughness and intersecting turbulent shear layers decays. For $R_{\text{bar}} > 245$, the turbulence self-sustains, causing the attachment-line flow, as well as the flow downstream of the attachment line, to become turbulent. In the absence of any contamination, the attachment line remains laminar, and viscous instability followed by rapid transition occurs only if $R_{\text{bar}} > 580$ (Ref. 19).

In the recent flight experiment, surface pressure measurements permit the calculation of R_{bar} for a given geometry and freestream conditions. (Note that the surface pressures are measured in the direction parallel to the centerline of the airplane.) The calculation procedure for R_{bar} is as follows. First, M and U are determined at each pressure port using the isentropic-flow equation, the measured port pressure, and freestream conditions. As a first approximation, the attachment line is estimated at the port location with the maximum pressure coefficient. At the attachment line, U_n is zero, and the sweep angle of the attachment line can be estimated from the expression for the spanwise velocity component where at the attachment line $W_\infty = U$. Next, U_n can be calculated for the other chord stations assuming locally infinite swept wing conditions where the ports on the lower surface (w.r.t. the attachment line) are assigned to have a negative velocity. In the vicinity of the attachment line of a swept infinite cylinder, the

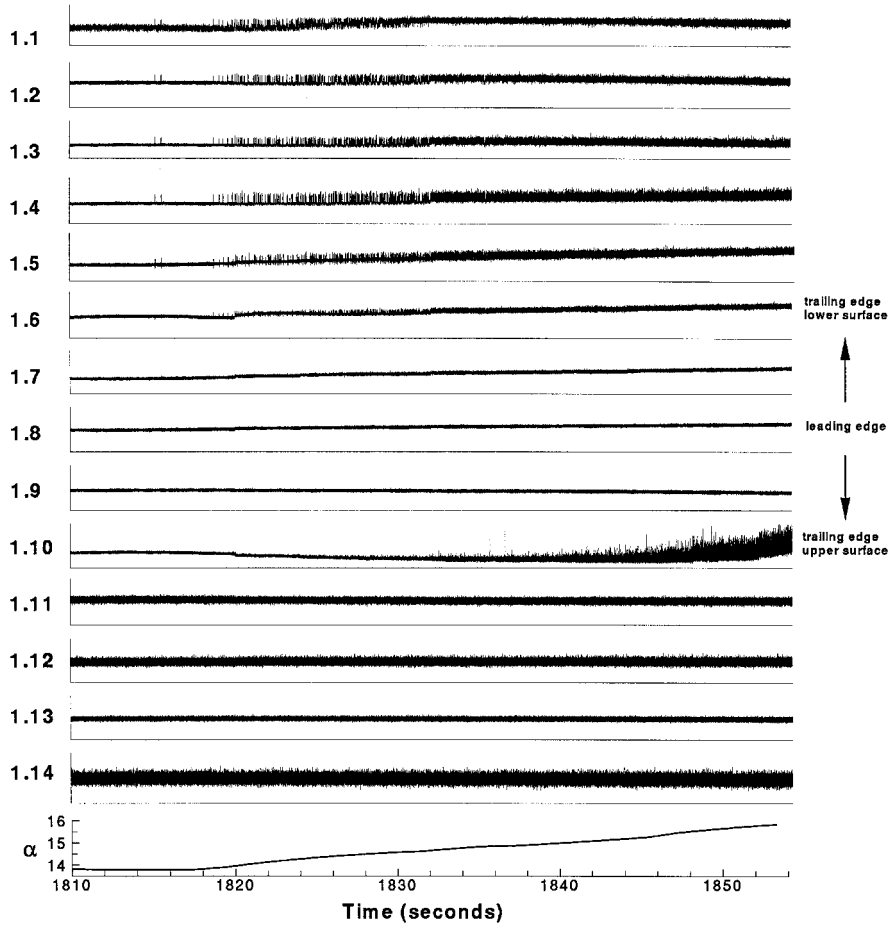

Fig. 7 Hot-film results (digital) depicting boundary-layer state changes on slat during slow deceleration (5-deg flaps, h_p = 5000 ft). Segment starts at t = 1810 s, α = 13.8 deg, M_∞ = 0.209, $R_{\bar{c}} = 14.5 \times 10^6$, and ends at t = 1854 s, α = 15.9 deg, M_∞ = 0.199, $R_{\bar{c}} = 13.7 \times 10^6$. Vertical scale range is identical for all sensors.

velocity normal to the attachment line is shown to be $U_n(s_n) = a_0 + a_1 s_n + a_3 s_n^3 + \ldots$, where s_n represents the distance along the surface normal to the attachment line ($s_n = 0$ at the leading edge of the slat and $s_n > 0$ on the upper surface).[20] Assuming that these conditions also locally exist in the leading-edge region of a lifting surface, then a least-squares fit of this expression through the U_n data in the vicinity of the attachment line provides an accurate estimate of the attachment-line location ($U_n = 0$) as well as the velocity gradient $U_n' = \mathrm{d}U_n/\mathrm{d}s_n$ at the attachment line.

This procedure was applied to calculate the slat attachment-line Reynolds number in slowly decelerating flight at constant altitude. In Fig. 8, the calculated values for R_{bar} are plotted as a function of angle of attack for the airplane in the 5-deg flaps configuration during three separate flights at h_p = 5000 ft (flight 707, run 2; flight 708, run 2; and flight 709, run 2). Note the good agreement between the curves providing additional evidence of the reliability of the results. The results show that R_{bar} remains well below 245 for the angle-of-attack range from about $\alpha \approx 3$ deg, the lowest angle of attack achievable in steady level flight at these conditions, to α = 9.5 deg. Between α = 9.5 and 12 deg, R_{bar} increases rapidly to a value of about 350 as the attachment line moves from the highly curved leading-edge region toward the relatively flat slat heel region on the lower surface. Correlation of the hot-film results of Fig. 7 and the calculated attachment-line Reynolds numbers indicates that on slat no. 5 the onset of attachment-line transition occurs at R_{bar} of about 340; significantly above the R_{bar} = 245 level for large disturbances. Note, this R_{bar} value was obtained for the high-lift system in the takeoff position; i.e., slat nos. 4 and 5 have identical positions with a sealed gap in between. The

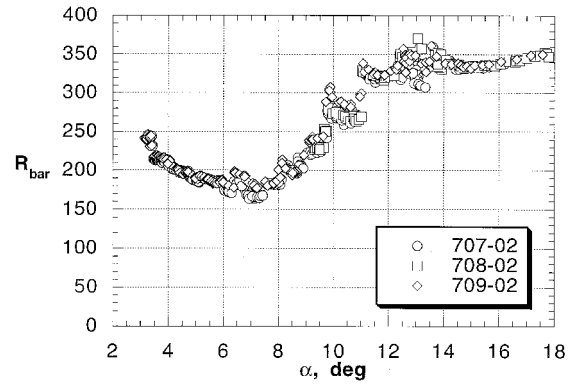

Fig. 8 Calculated attachment-line Reynolds number at WBL 324 (5-deg flaps, h_p = 5000 ft).

fact that attachment-line transition occurred at R_{bar} lower than the instability limit of 580 indicates that there likely was an effect of residual roughness because of the sealed flap gap and other spanwise discontinuities.

The signals of sensors 1.7–1.9 in Fig. 7 indicate that in the highly accelerated flow region around the leading edge, the turbulent flow appears to relaminarize. The upper surface suction peak occurred near sensor 1.9 and the signal of sensor 1.10 (Fig. 7) depicts a pattern (a drop in the mean signal value just before the rise in the mean value associated with transition) that is indicative of transition associated with laminar separation; another indication that the flow relaminarized. A convenient parameter often used to characterize the reversion

from turbulent to laminar flow is the inverse Reynolds number, $K = (U\zeta/\nu)^{-1}$, where the characteristic velocity is represented by the local inviscid velocity U, and $\zeta = U/U_s'$ represents the characteristic length. Here, U_s' denotes the velocity gradient along the inviscid streamline. Launder and Jones[21] and Narasimha and Sreenivasan[22] provide additional information on K. In two-dimensional flows, relaminarization is shown to occur for values of K in excess of approximately 3×10^{-6}. Very little data are available for three-dimensional wing flows; however, Beasley,[23] Hardy,[24] Arnal and Juillen,[25] and Meredith[15] suggest that a value of K in excess of 3×10^{-6} may also indicate relaminarization in three-dimensional wing flows if K is evaluated along the inviscid surface streamline.

Because U and ζ are inviscid-flow parameters, K can be calculated based on the measured surface pressures and the freestream conditions. The local edge velocity U is determined at every pressure port as explained earlier, and the velocity gradient along the inviscid streamline U_s' is calculated based on the normal velocity distribution U_n, the assumption that locally infinite swept-wing conditions exist, and the resulting calculated inviscid surface streamline. In Fig. 9, the maximum K value along the streamline is plotted as function of angle of attack for the 5-deg flap configuration during the identical runs used to calculate R_{bar}. Again, note the good agreement between the curves based on data obtained during different flights. The calculations indicate that K_{max} exceeds 3×10^{-6} for $\alpha = 5$ deg to stall onset ($\alpha = 18$ deg) and reaches a maximum value that is significantly larger than 3×10^{-6} at $\alpha \approx 9$ deg. This provides an additional indication that reversion to laminar flow was occurring in this initially turbulent slat flow as a result of the strong favorable pressure gradients. Earlier Preston-tube measurements reported by Yip et al.[6] indicate the likelihood of relaminarization of the slat flow in the high-lift configuration.

At low angles of attack ($\alpha < 7$ deg for 5-deg flaps and $\alpha < 5.5$ deg for 15-deg flaps), the attachment line was located on the upper surface just downstream of the leading edge and the pressure gradient along upper surface was favorable as shown in Fig. 4. However, the IR images, e.g., Fig. 6a for $\alpha = 2.9$ deg, as well as the hot-film results (Fig. 5), indicate that transition occurred upstream of the slat trailing edge at these conditions. In laminar-flow regions with a favorable pressure gradient, the growth of Tollmien-Schlichting disturbances is suppressed, but inflections in the mean velocity profile on swept wings give rise to crossflow vortices in the boundary layer. Provided that the attachment line is laminar, crossflow is the primary mode of laminar instability and transition for swept laminar-flow wings at cruise conditions. Consequently, the growth of these disturbances has been studied in great detail mainly using methods based on linear stability theory.[26] Vijgen et al.[27] were the first to study leading-edge flows along swept high-lift systems using linear stability methods, and their study shows that crossflow instability may also be a transition mechanism for these flows.

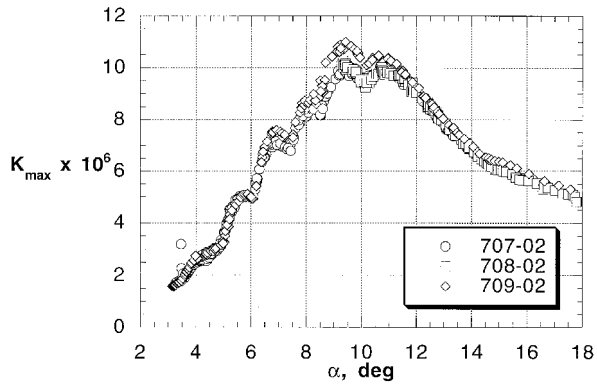

Fig. 9 Calculated maximum relaminarization parameter at WBL 324 (5-deg flaps, h_p = 5000 ft).

In this paper, the growth of the crossflow instabilities is analyzed using a linear stability method,[28] the flight measured surface pressures at WBL 324 and the freestream conditions. Integration of the crossflow amplification rates gives an amplification factor n, where $n = \ell n(A/A_0)$, with A representing the local integrated amplitude of the crossflow instability, and A_0 representing the initial amplitude at the neutral point. Here, the envelope method approach is used, whereby the local amplification rate is maximized by varying the wave-front angle and wavelength.[29] The three-dimensional mean velocity profiles required for the boundary-layer stability analysis were calculated using a compressible-flow method.[30] In Fig. 10, the predicted crossflow amplification along the upper surface of the slat is shown for a range of wave frequencies at three angles of attack: 1) Fig. 10a, $\alpha = 2.6$ deg ($M_\infty = 0.315$, $R_{\bar{c}} = 21.8 \times 10^6$), the lowest angle-of-attack that could be reached at the given weight and flight conditions (h_p = 5000 ft, 15-deg flaps); 2) Fig. 10b, $\alpha = 4.4$ deg ($M_\infty = 0.278$, $R_{\bar{c}} = 19.2 \times 10^6$), the angle of attack at which transition was observed to occur near the slat trailing edge; and 3) Fig. 10c, $\alpha = 7.0$ deg ($M_\infty = 0.244$, $R_{\bar{c}} = 16.9 \times 10^6$), the angle of attack for which the pressure gradient along the upper surface is fairly flat except near the leading edge. In all cases, the stationary crossflow instabilities ($f = 0$ Hz) are shown to amplify rapidly starting near the attachment line to $x/c \approx 0.2$. Depending on the pressure gradients, the growth rates along the remainder of the slat upper surface vary. Also, the traveling instabilities ($f > 0$ Hz) are shown to amplify stronger than the stationary instabilities in agreement with other subsonic analyses.[26] Although boundary-layer stability predictions based on linear theory indicate that traveling crossflow instabilities have larger growth rates than stationary instabilities and, thus, would be expected to dominate the transition process, experimental results have shown that stationary vortices tend to be dominant in quiet flows with low turbulence levels. In these flows, micron-size surface irregularities cause the initial amplitudes of the stationary disturbances to be significantly larger than those of the traveling disturbances, and this causes the domination of the stationary vortices in the transition process.[31] For the stationary instabilities, a maximum linear amplification factor n_{max} of 12 is predicted near the trailing edge at $\alpha = 4.4$ deg (Fig. 10b). At lower angles of attack, n_{max} for the stationary crossflow instabilities is predicted to be higher (Fig. 10a), and at higher angles of attack, n_{max} is predicted to be lower (Fig. 10c). Application of linear stability theory to predict swept-wing boundary-layer transition requires systematic correlations between transition-onset locations observed in similar experiments and calculated values for n_{max} at those locations. Application of this so-called e^n-transition prediction method to previous crossflow experiments has resulted in values for n_{max} at transition in the range of 9–12 (Ref. 26). The fact that in-flight the transition-onset location moved toward the trailing edge with increasing angle of attack and reached the trailing edge at $\alpha \approx 4.4$ deg, correlates well with these predicted trends in n_{max} (Fig. 10b), and indicates that crossflow instability was the likely cause of transition on the upper surface of the slat at the lower angles of attack.

In summary, the observed boundary-layer state phenomena on the deployed slat can be divided into three broad categories based on angle of attack. At low angles of attack, the attachment line is laminar and located on the upper surface of the slat. The ensuing leading-edge suction peak on the lower surface leads to transition just downstream of the peak as a result of rapid growth of Tollmien-Schlichting/inflection instabilities on the lower surface. On the upper surface, growth of crossflow instabilities in the favorable pressure gradient flow causes transition ahead of the trailing edge. In the mid angle-of-attack range, the attachment line is located near the leading edge and the pressure gradients on the upper and the lower surface are fairly flat, except near the leading edge. At these conditions, the flow over the entire slat is laminar (except for the separated

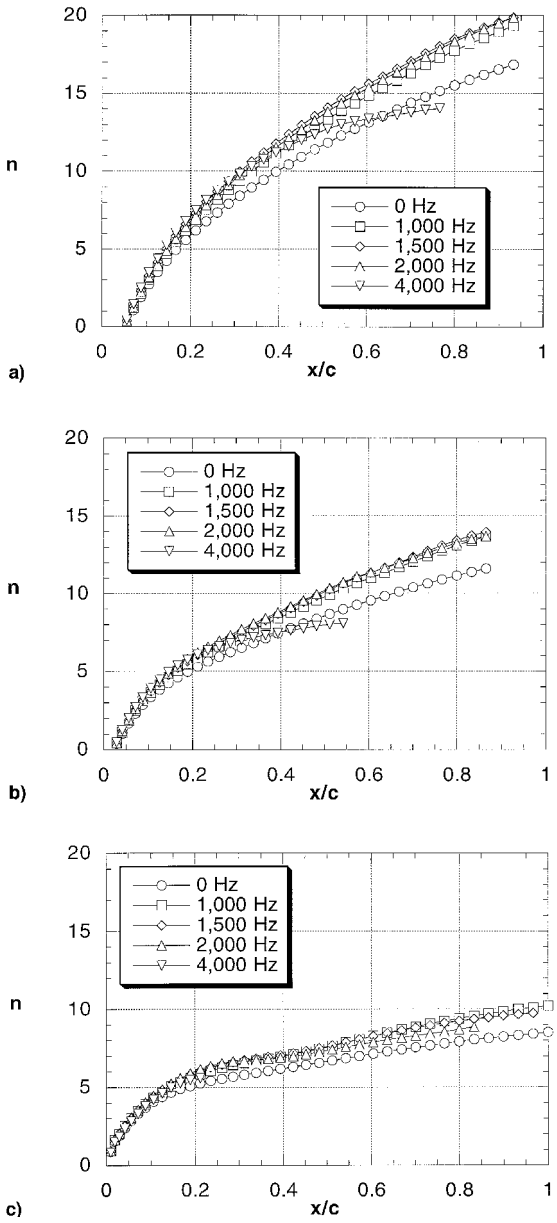

Fig. 10 Crossflow linear stability predictions (envelope method, crossflow only) for flow along upper surface of slat (15-deg flaps, h_p = 5000 ft): a) α = 2.6 deg, M_∞ = 0.315, $R_{\bar{c}}$ = 21.8 × 10^6; b) α = 4.4 deg, M_∞ = 0.278, $R_{\bar{c}}$ = 19.2 × 10^6; and c) α = 7.0 deg, M_∞ = 0.244, $R_{\bar{c}}$ = 16.9 × 10^6.

flow in the cove). At higher angles of attack, the attachment line moves away from the highly curved leading edge toward the relatively flat slat heel. This causes the attachment-line flow to become unstable and susceptible to contamination, and the lower-surface flow becomes turbulent at high angles of attack. Under the influence of the strong favorable pressure gradient leading to the suction peak on the upper surface, the flow reverses from the turbulent to a laminar state. Just downstream of the upper-surface suction peak, the relaminarized flow transitions as a result of rapid growth of Tollmien-Schlichting/inflectional instabilities or laminar separation. Note that under typical takeoff conditions, the airplane tends to operate in the mid- to high angle-of-attack range ($\alpha \approx 8$ deg).

Concluding Remarks

Flight experiments on NASA Langley Research Center's TSRV (B737-100) airplane have been conducted to document flow characteristics for further understanding of high-lift flows. Detailed boundary-layer state measurements conducted on the slat are analyzed and presented in this paper.

The hot-film and IR results validate earlier predictions that significant regions of laminar flow can exist in flight on the slat of a subsonic civil transport airplane at high-lift conditions. The analysis of the boundary-layer state changes observed in flight show that at high angles of attack, the transition process on the lower surface of the slat is governed by contamination of the attachment-line flow. Correlation of the surface-pressure data and the hot-film anemometer data indicates that attachment-line transition occurs at R_{bar} of approximately 340, well above the value of 245 for large disturbances. As a result of the strong favorable pressure gradients at typical high-lift conditions, K exceeds 3×10^{-6}, and the flow is shown to reverse to a laminar state in the slat leading-edge region. On the upper surface, the flow retransitions to the turbulent state under the influence of the adverse pressure gradient downstream of the leading-edge suction peak.

At low angles of attack, the laminar attachment line ($R_{bar} <$ 245) resides on the upper surface. The ensuing leading-edge suction peak on the lower surface causes transition governed by Tollmien-Schlichting/inflectional instabilities just downstream of the leading edge on the lower surface. In the favorable pressure gradient region on the upper surface, linear stability theory predicts amplification factors for stationary crossflow vortices in excess of 12. Amplification factors of this level have been correlated to crossflow transition, and the IR and hot-film data obtained in the high-lift experiment also show transition on the slat in the favorable pressure gradient region at these conditions.

Acknowledgments

The work by the following authors was supported by the NASA Langley Research Center under Cooperative Agreements NCC1-163 and NCC1-207 (van Dam and Los) and Contracts NAS1-19858 (Miley), NAS1-19864 (Bertelrud), and NAS1-19299 (Vijgen). The infrared imaging system was supplied by the Boeing Commercial Airplane Group under a Memorandum of Agreement with NASA. Also we would like to thank the Institute for Design Aerodynamics, German Aerospace Research Establishment in Braunschweig for their technical assistance with the mylar. The authors acknowledge the extraordinary efforts of Keith Harris and Jim Bartlett of the NASA Langley Research Center during the development and installation of the hot-film sensors and anemometry instrumentation.

References

[1]Fiddes, S. P., Kirby, D. A., Woodward, D. S., and Peckham, D. H., "Investigations into the Effects of Scale and Compressibility on Lift and Drag in the RAE 5m Pressurised Low-Speed Wind Tunnel," *Aeronautical Journal*, Vol. 89, March 1985, pp. 93–108.

[2]Greff, E., "In-Flight Measurement of Static Pressures and Boundary-Layer State with Integrated Sensors," *Journal of Aircraft*, Vol. 28, No. 5, 1991, pp. 289–299.

[3]Thibert, J. J., "The Garteur High Lift Research Programme," *High-Lift System Aerodynamics*, CP-515, AGARD, Sept. 1993, pp. 16-1–16-21.

[4]Yip, L. P., Vijgen, P. M. H. W., and Hardin, J. D., "In-Flight Surface-Flow Measurements on a Subsonic Transport High-Lift System," International Council of Aeronautical Sciences, Paper 92-3.7.3, Sept. 1992.

[5]Yip, L. P., Vijgen, P. M. H. W., Hardin, J. D., and van Dam, C. P., "In-Flight Pressure Distributions and Skin-Friction Measurements on a Subsonic Transport High-Lift Wing Section," *High-Lift System Aerodynamics*, CP-515, AGARD, Sept. 1993, pp. 21-1–21-19.

[6]Yip, L. P., Vijgen, P. M. H. W., Hardin, J. D., and van Dam, C. P., "In-Flight Pressure Measurements on a Subsonic Transport High-Lift Wing Section," *Journal of Aircraft*, Vol. 32, No. 3, 1995, pp. 529–538.

[7]Yip, L. P., van Dam, C. P., Whitehead, J. H., Hardin, J. D., Miley, S. J., Potter, R. C., Bertelrud, A., Edge, D. C., and Willard, P. E.,

"The NASA B737-100 High-Lift Flight Research Programme-Measurements and Computations," *Aeronautical Journal*, Vol. 99, Nov. 1995, pp. 372–386.

[8]Van Dam, C. P., Los, S. M., Miley, S. J., Roback, V. E., Yip, L. P., Bertelrud, A., and Vijgen, P. M. H. W., "In-Flight Boundary-Layer State Measurements on a High-Lift System: Main Element and Flap," *Journal of Aircraft*, Vol. 34, No. 6, 1997, pp. 757–763.

[9]Kline, S. J., and McClintock, F. A., "Describing Uncertainties in Single-Sample Experiments," *Mechanical Engineering*, Vol. 75, Jan. 1953, pp. 3–8.

[10]Brandon, J. M., Manuel, G. S., Wright, R. E., and Holmes, B. J., "In-Flight Visualization Using Infrared Imaging," *Journal of Aircraft*, Vol. 27, No. 7, 1990, pp. 612–618.

[11]Horstmann, K. H., Redeker, G., Quast, A., Dressler, U., and Bieler, H., "Flight Tests with a Natural Laminar Flow Glove on a Transport Aircraft," AIAA Paper 90-3044, Aug. 1990.

[12]Crowder, J. P., "Infrared Cameras for Detection of Boundary Layer Transition in Transonic and Subsonic Wind Tunnels," AIAA Paper 90-1450, June 1990.

[13]Miley, S. J., van Dam, C. P., Yip, L. P., Willard, P. E., Crowder, J. P., and Wazlavick, R. L., "Slat Transition Characteristics on the NASA B737-100 Aircraft using Infrared Imaging and Hot-Film Anemometry," *Flow Visualization VII*, edited by J. Crowder, Begell House, New York, 1995, pp. 950–956.

[14]Woodward, D. S., Hardy, B. C., and Ashill, P. R., "Some Types of Scale Effect in Low-Speed High-Lift Flows," International Council of Aeronautical Sciences Paper 4.9.3, Aug. 1988.

[15]Meredith, P. T., "Viscous Phenomena Affecting High-Lift Systems and Suggestions for Future CFD Development," *High-Lift System Aerodynamics*, CP-515, AGARD, Sept. 1993, pp. 19-1–19-8.

[16]Gaster, M., "On the Flow Along Swept Leading Edges," *Aeronautical Quarterly*, Vol. 18, May 1967, pp. 165–184.

[17]Pfenninger, W., "Laminar Flow Control Laminarization, USAF and NAVY Sponsored Northrop LFC Research Between 1949 and 1967," *Special Course on Concepts for Drag Reduction*, AGARD Rept. 654, March 1977, pp. 3-1–3-75.

[18]Poll, D. I. A., "Transition in the Infinite-Swept Attachment-Line Boundary-Layer," *Aeronautical Quarterly*, Vol. 30, Pt. 4, Nov. 1979, pp. 607–629.

[19]Hall, P., Malik, M. R., and Poll, D. I. A., "On the Stability of an Infinite Swept Attachment Line Boundary Layer," *Proceedings of the Royal Society of London, Series A: Mathematical and Physical Sciences*, Vol. 395, 1984, pp. 229–245.

[20]Crabtree, L. F., Küchemann, D., and Sowersby, L., "Three-Dimensional Boundary Layers," *Laminar Boundary Layers*, edited by L. Rosenhead, Oxford Univ. Press, Oxford, England, UK, 1963, pp. 409–491.

[21]Launder, B. E., and Jones, W. P., "On the Prediction of Relaminarization," Aeronautical Research Council, CP 1036, Feb. 1968.

[22]Narasimha, R., and Sreenivasan, K. R., "Relaminarization of Fluid Flows," *Advances in Applied Mechanics*, edited by Chia-Shun Yih, Vol. 19, Academic Press, New York, London, 1979, pp. 221–309.

[23]Beasley, J. A., "Calculation of the Laminar Boundary Layer and Prediction of Transition on a Sheared Wing," Aeronautical Research Council, R&M 3787, Oct. 1976.

[24]Hardy, B. C., "Experimental Investigation of Attachment-Line Transition in Low-Speed High-Lift Wind-Tunnel Testing," *Fluid Dynamics of Three-Dimensional Turbulent Shear Flows and Transition*, CP-438, AGARD, 1988, pp. 2-1–2-17.

[25]Arnal, D., and Juillen, J. C., "Leading-Edge Contamination and Relaminarization on a Swept Wing at Incidence," *Numerical and Physical Aspects of Aerodynamic Flows IV*, edited by T. Cebeci, Springer–Verlag, Berlin, 1990, pp. 391–402.

[26]Reed, H. L., and Saric, W. S., "Linear Stability Theory Applied to Boundary Layers," *Annual Review of Fluid Mechanics*, Vol. 28, 1996, pp. 389–428.

[27]Vijgen, P. M. H. W., Hardin, J. D., and Yip, L. P., "Flow Prediction over a Transport Multi-Element High-Lift System and Comparison with Flight Measurements," 5th Symposium on Numerical and Physical Aspects of Aerodynamic Flows, California State Univ., Long Beach, CA, Jan. 1992.

[28]Malik, M. R., "COSAL—A Black-Box Compressible Stability Analysis Code for Transition Prediction in Three-Dimensional Boundary Layers," NASA CR 165925, May 1982.

[29]Malik, M. R., "Stability Theory for Laminar Flow Control Design," *Viscous Drag Reduction in Boundary Layers*, edited by D. Bushnell and J. Hefner, Vol. 123, Progress in Astronautics and Aeronautics, AIAA, Washington, DC, 1990, pp. 3–36.

[30]Wie, Y. S., "BLSTA—A Boundary-Layer Code for Stability Analysis," NASA CR 4481, Dec. 1992.

[31]Reibert, M. S., Saric, W. S., and Carrillo, R.B., Jr., "Experiments in Nonlinear Saturation of Stationary Crossflow Vortices in a Swept-Wing Boundary Layer," AIAA Paper 96-0184, Jan. 1996.